Proceedings of the
Annual Stability Conference
Structural Stability Research Council
Orlando, Florida, April 12-15, 2016

Stability of Buried Corrugated Metal Pipe

P. Graham Cranston[1], Matthew C. Richie[2], Luiz C. M. Vieira, Jr[3]

Abstract
Stability of flexible pipe relies on support from the surrounding soil. For corrugated profiles, local and distortional buckling of corrugations can limit the capacity of the pipe. This paper presents current design methods for evaluating stability of buried corrugated metal pipe (CMP), and a parametric finite element analysis. Soil support is included in the finite element analysis and its effect on the stability of the pipe is explored. The study covers a range of typical diameters, profiles, and soil stiffnesses. The results of the parametric finite element analysis are presented, and the global, local, and distortional stability of CMP is discussed. We find that soil support has a significant effect on the global stability of buried CMP, but comparatively less of an effect on the local and distortional buckling modes as smaller displacements fail to mobilize the resistance of the soil.

Keywords: Corrugated metal pipe (CMP), Buried pipe, Structural stability, Finite element analysis, Buckling.

1. Introduction
Corrugated metal pipe (CMP) gained popularity as highway culvert pipes in the late 1950s, coincident with the expansion of the U.S. highway system. CMP is available in a variety of shapes and sizes ranging from 6 inch (150 mm) round pipe to arches spanning over 80 feet (24 m), and it currently exists in innumerable installations such as buried bridges, culverts, grade separations, and storm drain systems. The appeal of CMP lies in its versatility, ease of handling, and relative low cost for a given strength of pipe. The corrugated profile adds strength while reducing wall thickness, but the majority of design efficiencies comes from interaction between the pipe and the soil.

CMP is classified as flexible pipe, which relies heavily on support from the surrounding soil to carry load. The design of buried flexible pipe is often governed by stability. Global stability of flexible pipe is a function of the support provided by the soil-structure system and can vary greatly with the quality of the installation. Current design codes for CMP include global stability limit states as a function of soil stiffness, and limits on out-of-roundness are also specified. Local or distortional stability limits are not typically considered by design codes, and interaction between local/distortional and global buckling modes is not addressed. Instead, standardized corrugation profiles which are intended to minimize the potential for local buckling are specified.

This study contributes to the body of research on stability of CMP through a finite element analysis of the annular profiles defined in ASTM A796. This paper presents the results and conclusions of this work, preceded by background on the topic. The background section includes a brief literature review and

[1] S.E., M.ASCE, Simpson Gumpertz & Heger Inc., <prgcranston@sgh.com>
[2] P.E., M.ASCE, Simpson Gumpertz & Heger Inc., <mcrichie@sgh.com>
[3] Assistant Professor, University of Campinas, <vieira@fec.unicamp.br>

summary of current design code provisions for evaluating stability of buried corrugated metal pipes. We present results of our numerical studies which included analyses of compression of prismatic profiles, buckling of circular profiles, and analyses of surcharge loading on buried circular profiles. The interaction of global and local stability is also investigated. The results are compared with the design code provisions.

2. Current Design Methods

Pipe is classified structurally as either rigid or flexible structures. Rigid pipe is stiff and does not deflect appreciably without structural distress. Flexible pipe derives much of its structural integrity from the surrounding backfill, allowing for thinner walls and efficient use of materials. Flexible pipe has relatively low bending stiffness and low bending strength without soil support. Under external load, the vertical diameter decreases and the horizontal diameter increases, pushing into the backfill along the sides. The increase in horizontal diameter is resisted by the lateral soil pressure of the compacted side fill.

Flexible pipe can typically accommodate deflections of 2% to 7% of the pipe diameter without structural damage. Because flexible pipe, such as CMP, takes advantage of thinner walls it can be susceptible to buckling under compressive loads. Various design codes are available to the designer with different implementations of stability checks for corrugated steel pipe. A summary of the current code stability checks, and their differences, are presented below. Not mentioned below are other factors that influence the implementation of these code equations, including treatment of load factors and calculation of the soil prism. In spite of the differences outlined here, the various codes produce similar designs.

AASHTO

AASHTO LRFD Bridge Design Specifications (2014) require flexible metal pipe to be designed for thrust (ring compression), buckling strength, and seam resistance (if applicable). In design practice, wall area is first determined based on thrust. Buckling is then checked by comparing the yield strength of the wall to the critical buckling stress. AASHTO employs two equations for buckling based on a limiting diameter. The first equation represents interaction of buckling and yielding (plastic buckling):

$$if\ S < \left(\frac{r}{k}\right)\sqrt{\frac{24\,E_m}{F_u}}\ ,\qquad then\ f_{cr} = F_u - \frac{\left(\frac{F_u\,k\,S}{r}\right)^2}{48\,E_m} \tag{1}$$

For larger diameters, the following elastic buckling equation is used:

$$if\ S > \left(\frac{r}{k}\right)\sqrt{\frac{24\,E_m}{F_u}}\ ,\qquad then\ f_{cr} = \frac{12\,E_m}{\left(\frac{k\,S}{r}\right)^2} \tag{2}$$

where:
S = diameter of pipe or span of plate structure (in.)
E_m = modulus of elasticity (ksi)
F_u = tensile strength of metal (ksi)
f_{cr} = critical buckling stress (ksi)
r = radius of gyration of the pipe wall (in.)
k = soil stiffness factor taken as 0.22.

AASHTO states that the use of 0.22 for the soil stiffness is thought to be conservative for the types of backfill material allowed for pipe and arch structures, and that this lower bound has a long history of use in prior editions.

If the critical buckling stress is less than allowable stress based on thrust, wall area is recalculated based on f_{cr}. AASHTO also sets a lower bound on flexibility, the flexibility factor, to prevent damage and deformation during handling and installation.

For long-span culverts, AASHTO does not include a buckling limit state. Long-span metal culverts are defined by AASHTO as structural plate pipe and arch shapes that require the use of special features (continuous longitudinal stiffeners or reinforcing ribs), or special shapes of any size having a radius of curvature greater than 13 ft in the crown or side plates (except metal box culverts). Studies (McGrath et al., 2002) have shown that buckling theories for flexible pipe are excessively conservative and not controlling for long span structures; therefore, they were dropped from AASHTO code.

ASTM A796

Structural design guidelines for corrugated metal structures are provided in ASTM A796 Standard Practice for Structural Design of Corrugated Steel Pipe, Pipe-Arches, and Arches for Storm and Sanitary Sewers and Other Buried Application. These guidelines for buckling follow the method presented in AASHTO specifications.

NCSPA Design Manual

The American Iron and Steel Institute (AISI) developed a design method for corrugated steel pipe in 1967. This design method has since been updated and is included in the NCSPA Corrugated Steel Pipe Design Manual, which is available from the National Corrugated Steel Pipe Association (NSCPA). Buckling criteria are provided in three equations which represent yielding of the pipe wall, an interaction of yielding and ring buckling, and ring buckling alone. Ultimate compressive stress f_b is given by the following equations:

$$f_b = f_y \qquad where\ \frac{D}{r} \leq 294 \tag{3}$$

$$f_b = 40{,}000 - 0.081\left(\frac{D}{r}\right)^2 \qquad where\ 294 < \frac{D}{r} \leq 500 \tag{4}$$

$$f_b = \frac{4.93\ x\ 10^9}{\left(\frac{D}{r}\right)^2} \qquad where\ \frac{D}{r} > 500 \tag{5}$$

where: D = diameter or span (in.)
r = radius of gyration of the pipe wall (in.)

The NCSPA equations assume the yield strength f_y of CMP is 33 ksi (227.5 MPa) and an elastic modulus of 29,000 ksi (200 GPa). Substituting these values, Eq. 5 can be shown to be equivalent to the AASHTO equation for ring buckling (Eq. 2) for a soil stiffness factor $k = 0.266$.

Canadian Highway Bridge Design Code (CHBDC)

The CHBDC contains provisions for the design of buried structures, including flexible structures that depend on soil support (referred to as soil-steel structures) and metal box structures. The CHBDC design method provides guidance on thrust and buckling resistance, similar to AISI and AASHTO, but based on ultimate strength principles rather than working stress or service load design.

$$For\ R \leq R_e\ , \qquad f_b = F_m\left(F_y - \frac{\left(F_y\ K\ R\right)^2}{12\ E\ r^2\ \rho}\right) \tag{6}$$

$$For\ R > R_e\ , \qquad f_b = \frac{3\,\rho\,F_m\,E}{\left(\frac{K\,R}{r}\right)^2} \tag{7}$$

where: f_b = ultimate compressive stress (MPa)
F_y = yield strength (MPa)
R = radius of curvature of wall (mm)
r = radius of gyration of the corrugation profile (mm)
$R_e = \frac{r}{K}\left[\frac{6E\rho}{F_y}\right]^{0.5}$ is the equivalent radius (mm)
K = factor representing relative stiffness of the pipe and surrounding soil

F_m and ρ are factors that account for the presence of closely spaced conduits and low cover, respectively. These effects are not considered in the present study. CHBDC also differs from AASHTO and AISI in that it uses a combined bending and axial strength check in lieu of a flexibility factor for handling and installation.

Comparison

The compressive stress limits specified by each of the three codes discussed are shown in Figure 1. The values for CHBDC are plotted assuming a fixed K = 0.233 to facilitate the comparison, though CHBDC specifies a more detailed calculation for the effect of soil support as a function of soil stiffness, while AASHTO and NCSPA specify requirements on the backfill and installation, and use a conservative value for k. The AASHTO equations are based on the ultimate strength while the other two codes are based on yield strength, and as a result the nominal compressive stress limit in AASHTO is higher.

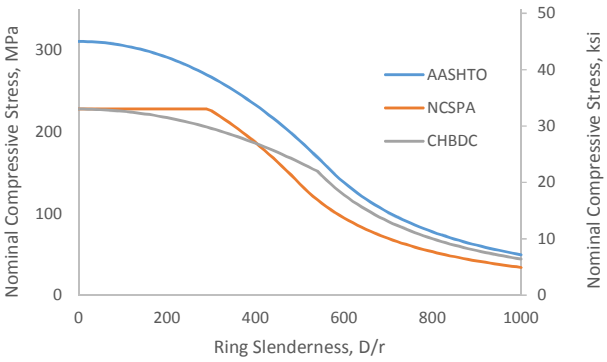

Figure 1 - Comparison of design code compressive stress limits

3. Research into stability of buried flexible pipes

Luscher (1966) studied the buckling behavior of tubes surrounded by soil and showed that the surrounding soil significantly increases the buckling capacity as compared to an unsupported pipe. His research used discrete springs of uniform stiffness around the pipe circumference. Luscher's buckling equation (8) is currently used in AASHTO specifications for thermoplastic pipe.

$$p_{cr} = \frac{2\,B\,R_w\,M_s\,E\,I^3}{R^{1.5}} \tag{8}$$

where B is dimensionless nonuniform stress distribution factor, M_s is the soil constrained modulus, and R_w is a water buoyancy factor.

Duns and Butterfield (1971) derived a set of equations to predict the elastic critical load of buried thin-walled cylinders; the equations were shown to be in close agreement with experimental results. The same research topic was later explored in Moore (1989), which presented an extensive review of test data available at the time, and compared the results with analyses that include soil support for flexible pipes by both equivalent springs (i.e., a Winkler foundation) and a continuum representation of the soil. Moore (1989) also presented the following equation for the global critical springline thrust N_{ch} for flexible cylinders of radius R, flexural stiffness EI, and elastic soil stiffness $E_s^\star$:

$$N_{ch} = \frac{(n^2 - 1)EI}{R^2} + \frac{E_s^{\star} R}{2n + (1 - 2\nu_s)/(1 - \nu_s)} \tag{9}$$

The above equation is minimized for harmonic wave number n. Analysis of the data collected found that a correction factor of 0.55 should be applied to the analytical critical thrust to align with test results.

Moore et al. (1989) also presented an analytical analysis of different combinations of pipe configuration and loading. They further propose adjustment factors for layered soil profiles and non-circular cross-sections. In this treatment of global stability, the pipes are treated as solid walls and stability depends only on moment of inertia.

Moore (1994) showed that Winkler foundation idealizations of buried pipe (pipe supported on equivalent springs around the circumference) were too conservative. They concluded that modeling soil support as continuous changes the relative contribution of soil and pipe to the buckling capacity, and increases the capacity predicted for large-span culverts to better agree with test results. Moore asserted that buckling design based on the continuum theory provides a better approximation. In terms of critical buckling stress, Moore (1994) proposed:

$$p_{cr} = \frac{1.2\ C_n\ M_s\ {K_b}^{2/3}\ E\ I^{1/3} R_h}{R} \tag{10}$$

where C_n is a scalar calibration factor to account for nonlinear effects and R_h accounts for nonuniformity of ground support.

In NCHRP Report 473, McGrath et al (2002) proposed modification to AASHTO design practice for long-span metal culvert that included a recommendation to include a buckling check based on Moore's continuum equation. McGrath et al (2002) noted that "the current AASHTO design equation considers pipe and soil stiffness in the term $(M_s EI)^{0.5}/R^{1.5}$, whereas the continuum theory considers the pipe stiffness with the term $(EI)^{1/3}\ M_s^{2/3}/R$. This formulation has the effect of decreasing the importance of pipe stiffness, increasing the importance of soil stiffness, and, perhaps most importantly, reducing the influence of the radius from $1/R^{1.5}$ to $1/R$. The latter term, which derives from the use of continuous support instead of discreet springs, results in increased predicted buckling capacity for large-span culverts."

Stability under extreme loads has also been a topic of research on buried pipes. Uckan et al. (2015) recently presented a numerical study on the seismic response of buried steel pipes at fault crossings. Important conclusions were obtained; however, the study did not consider buckling of the steel pipe. Trickey et al. (2015) carried out a parametric study of frost-induced bending moments in buried cast iron water pipes.

As older buried pipes reach their expected service lives, researchers have been concerned with methods and techniques to assess damage and to retrofit the damaged pipes. Wilson et al. (2015) analyzed the probability of failure of large-diameter aged cast iron pipes. García and Moore (2015) conducted laboratory testing to study the performance of rehabilitated steel culverts. Brown et al. (2014) examined through finite element models the performance of a cured-in-place pipe. Zhang et al. (2014) presented a very complete study on integrity assessment and safety evaluation of buried steel pipes; the study used the extended finite element method (XFEM) and results were compared with standards, previous studies, and experiments.

Table 1 - Corrugation profiles analyzed. Collected from annular profiles defined in ASTM A796.

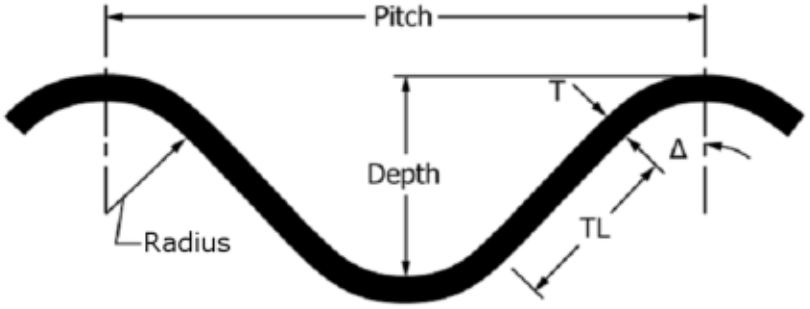

Profile Dimensions	Profile ID	Thickness mm	TL mm	Δ Degrees	Area mm2/mm	Moment of mm4/mm	Radius of mm
Pitch: 67.7 mm Depth: 12.7 mm Radius: 17.5 mm (Class 1, Table 5)	1	1.02	19.9	26.56	0.984	18.39	4.232
	2	1.32	19.8	26.65	1.31	24.58	4.336
	3	1.63	19.6	26.74	1.64	31	4.348
	4	2.01	19.3	26.86	2.049	39.2	4.371
	5	2.77	18.8	27.11	2.87	56.13	4.422
	6	3.51	18.3	27.37	3.691	74.28	4.486
	7	4.27	17.8	27.65	4.515	93.82	4.559
Pitch: 76.2 mm Depth: 25.4 mm Radius: 14.3 mm (Class 2, Table 7)	8	1.32	24.2	44.39	1.505	112.94	8.661
	9	1.63	23.8	44.6	1.884	141.88	8.679
	10	2.01	23.4	44.87	2.356	178.34	8.705
	11	2.77	22.6	45.42	3.302	253.31	8.758
	12	3.51	21.7	46.02	4.25	330.61	8.819
	13	4.27	20.8	46.65	5.203	411.04	8.887
Pitch: 125.0 mm Depth: 26.0 mm Radius: 40.0 mm (Class 3, Table 9)	14	1.63	18.5	35.58	1.681	145.03	9.289
	15	2.01	18	35.8	2.1	181.77	9.304
	16	2.77	16.9	36.3	2.942	256.46	9.34
	17	3.51	15.6	36.81	3.785	332.94	9.38
	18	4.27	14.3	37.39	4.627	411.18	9.426
Pitch: 152.4 mm Depth: 50.8 mm Radius: 28.6 mm (Class 4, Table 33)	19	2.82	48.08	44.47	3.294	990.06	17.3
	20	3.56	47.27	44.73	4.24	1280.93	17.4
	21	4.32	46.43	45	5.184	1575.89	17.4
	22	4.79	45.9	45.18	5.798	1769.8	17.5
	23	5.54	45.03	45.47	6.771	2079.8	17.5
Pitch: 152.4 mm Depth: 50.8 mm Radius: 28.6 mm (Class 4, Table 33)	24	6.32	44.15	45.77	7.743	2395.25	17.6
	25	7.11	43.23	46.09	8.719	2717.53	17.7
	26	8.08	41.99	46.47	9.887	3113.54	17.7
	27	9.65	40.16	47.17	11.881	3801.8	17.9
Pitch: 381 mm Depth: 139.7 mm Radius: 76.2 mm (Class 5, Table 35)	28	3.56	110.8	49.75	4.784	11710.7	49.48
	29	4.32	109.8	49.89	5.846	14332.5	49.5
	30	4.79	109.2	49.99	6.536	16037	49.53
	31	5.54	108.2	50.13	7.628	18740.1	49.58
	32	6.32	107.2	50.28	8.716	21441.2	49.61
	33	7.11	106.1	50.43	9.807	24124.5	49.63
Pitch: 500 mm Depth: 237 mm Radius: 80 mm (Class 6, Table 37)	34	7.11	198.8	55.7	10.627	70803.75	81.62
	35	8.1	197.6	55.8	12.144	81036.1	81.69
	36	9.65	195.6	55.9	14.509	97031.45	81.78

4. Finite Element Analysis

We developed three sets of FE models to investigate the stability of buried CMP. The following sets of analyses were performed:

- Plane strain (2D) analyses of linear-elastic eigenvalue global buckling of buried CMP to evaluate global stability.
- Linear-elastic eigenvalue buckling of straight corrugated profiles of varying length without soil support to evaluate local and distortional stability (see Figure 5).
- Nonlinear compression to collapse of straight corrugated profiles of varying length without soil support to evaluate local and distortional stability and post-buckling response.

The models were developed in ABAQUS v6.14-1 (2014) and use parametric input file definitions to quickly generate the mesh for each profile, diameter/length, and surrounding soil, as applicable. The profiles analyzed are shown in Table 1. The analysis sets comprise all profiles and a broad range of diameters/heights and soil stiffnesses far exceeding typical installation conditions. Throughout the discussion, two profiles are used as examples to highlight certain behavior: Profiles 8 and 13. These profiles have the same pitch, depth, and radius of curvature or the crests, but are at the extremes of thickness for their class (Class 2).

4.1. Global Stability

The global stability of the pipe-soil system is evaluated by 2D plane strain linear eigenvalue analysis of a buried pipe and surrounding soil. The set of analyses comprised the 36 profiles under consideration, each at eleven diameters (logarithmically spaced) and at eleven soil stiffnesses (logarithmically spaced), for a total of 4356 analysis runs. The diameters were selected to be plus-or-minus one order of magnitude from the approximate transition between yield-controlled and stability-controlled responses as defined by AASHTO and ASTM A796, presented above as Equations 1 and 2.

The pipe is modeled using two-node linear beam elements B21 at the centroid of the profile, with equivalent area and moment of inertia. The surrounding soil is modeled with four-node plane strain elements CPE4. The mesh density was such that a minimum of six beam elements were included over each half-wavelength of the pipe wall in the highest mode extracted, and in most cases eight or more beam elements were included over a half-wave.

The soil mass extends out ten diameters from the pipe, and test runs found this distance to be sufficient to eliminate boundary effects. Soil elastic modulus was varied plus-or-minus one order of magnitude from 26 MPa. The pipe and soil are assumed to be fully bonded, and neither separation nor sliding are permitted. Provided that sufficient soil cover exists to provide positive pressure around the entirety of the pipe, the assumption of no separation is valid for predicting the onset of buckling, until significant post-buckling displacements occur. The assumption of no sliding is necessary for linear eigenvalue analyses, which cannot represent the nonlinear behavior of frictional sliding.

The pipes were subjected to a unit external positive pressure, and the first ten eigenvalue buckling modes were extracted. Figure 2 above plots the critical buckling pressure against the number of buckling waves around the circumference and also shows the normalized deformed shapes for the modes plotted.

The global buckling response of the pipe-soil system is a balance between the bending stiffness of the pipe, and the radial stiffness of the surrounding soil. For typical construction, the flexible pipe may be treated as inextensional. As a result, the mode shapes expressed as a fraction of the radius were the same for all analyses, and only the critical load for each mode varied. Note that the extent of soil deformation is higher for lower harmonic number modes, and vice versa. Alternatively, it can be said that at lower harmonic wave

numbers, the greater proportion of strain energy in the system is soil strain energy while at higher harmonic wave numbers the greater proportion of strain energy in the system is pipe strain energy.

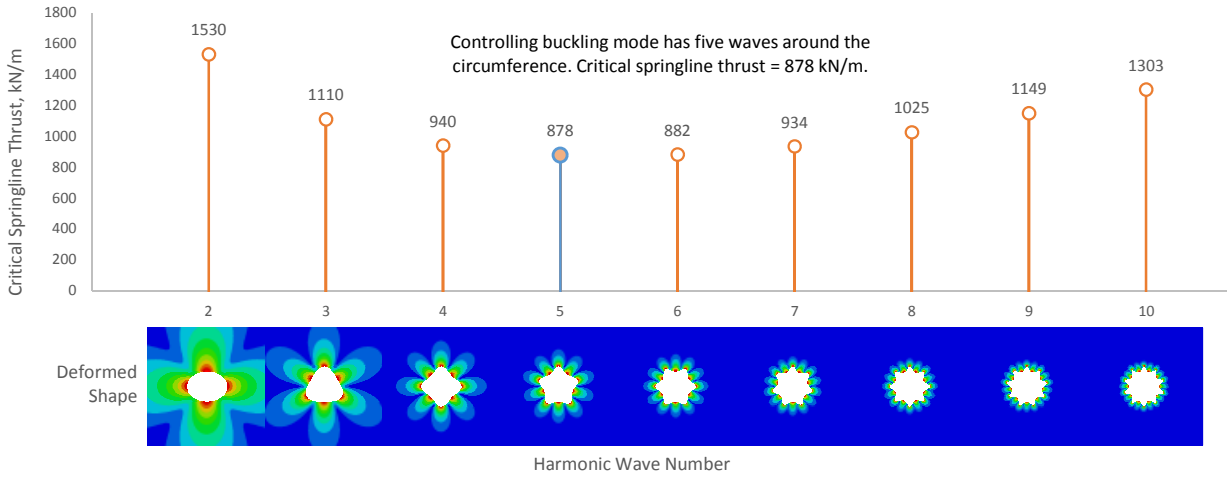

Figure 2 – Critical buckling springline thrust for harmonic wave numbers two through ten.
Profile geometry: pitch 67.7 mm; depth 12.7 mm; thickness 4.27 mm; diameter 2788 mm.
Soil parameters: elastic modulus 4.13 MPa; Poisson's ratio 0.28.

Extending this concept, local and distortional buckling modes of corrugated profiles have shorter wavelengths than global modes, as will be seen in the following section. Buckling modes with short wavelengths, accompanied by smaller deflections compared with global modes, are expected to be only weakly influenced by soil support. This phenomenon is discussed further in Sec. 4.2.

The critical external pressure for the controlling global buckling mode in each analysis is plotted against ring bending stiffness EI/R^3 in Figure 3. The results are colorized by the stiffness of the surrounding soil. There are two clear regimes of behavior. On the left side of the plot, at low ring bending stiffness, the critical pressure forms a family of parallel curves on the log-log plot as a function of soil elastic modulus. On the right side of the plot, the critical pressure converge and the effect of soil stiffness on the critical pressure vanishes. For high soil stiffness and low ring bending stiffness, at the upper left portion of the plot, the critical pressure predicted by FEA departs from the parallel family of log-log curves found at lower soil stiffnesses. The cause of this apparent increase in critical pressure is not yet known.

Figure 4 shows the same results colorized by controlling wave number. The plot shows that the number of waves for the controlling mode increases with increasing soil elastic modulus and/or with decreasing ring bending stiffness. On the right-hand side of the plot the controlling mode always has two waves and the effect of soil stiffness on critical pressure is diminished. In fact, if one calculated the wavelength of a straight beam on elastic foundation, the wavelength would be longer than πR. That is, the pipe when unconstrained by cyclic symmetry would have fewer than 2 waves over the arc length $2\pi R$, and the result for the circular pipe is to increase the global buckling capacity.

4.2. Local and Distortional Stability

To evaluate the local and distortional stability of CMP, we analyze in this section linear eigenvalue buckling and nonlinear load-displacement models of straight sections under axial compression without soil support. The sets of analyses comprised the 36 profiles under consideration, each at eleven heights (logarithmically spaced), for a total of 396 analysis runs in each set.

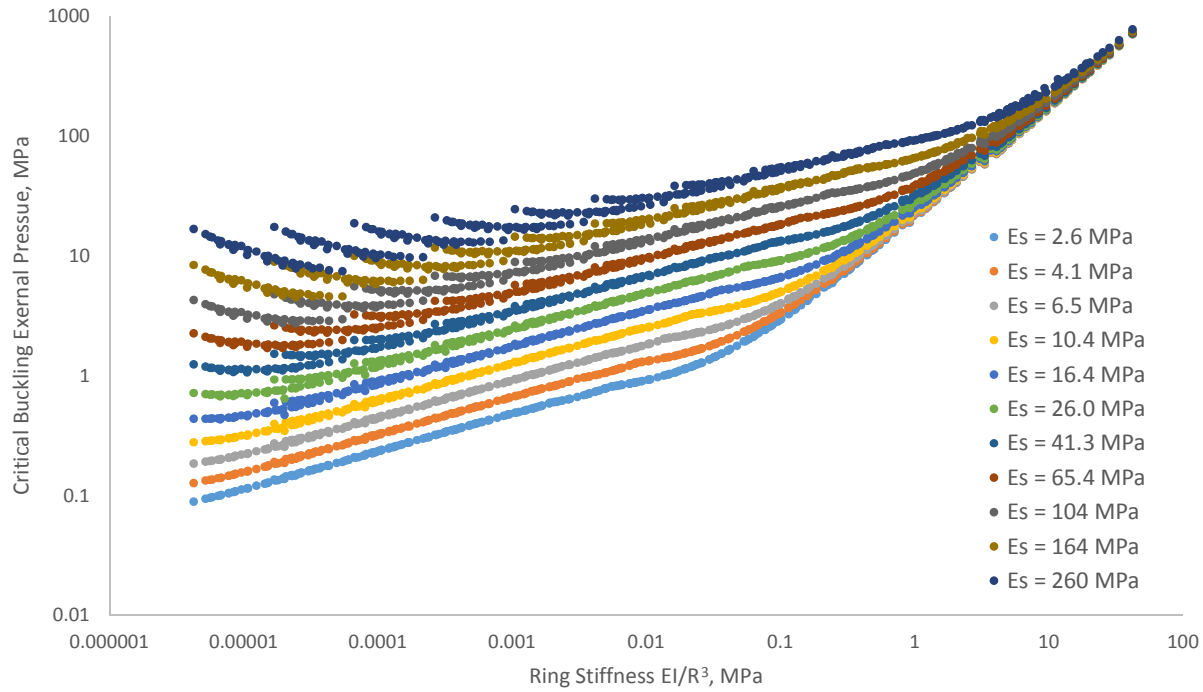

Figure 3 – Critical buckling pressure of circular pipes with elastic soil support, colorized by soil elastic modulus between 2.6 and 260 MPa.

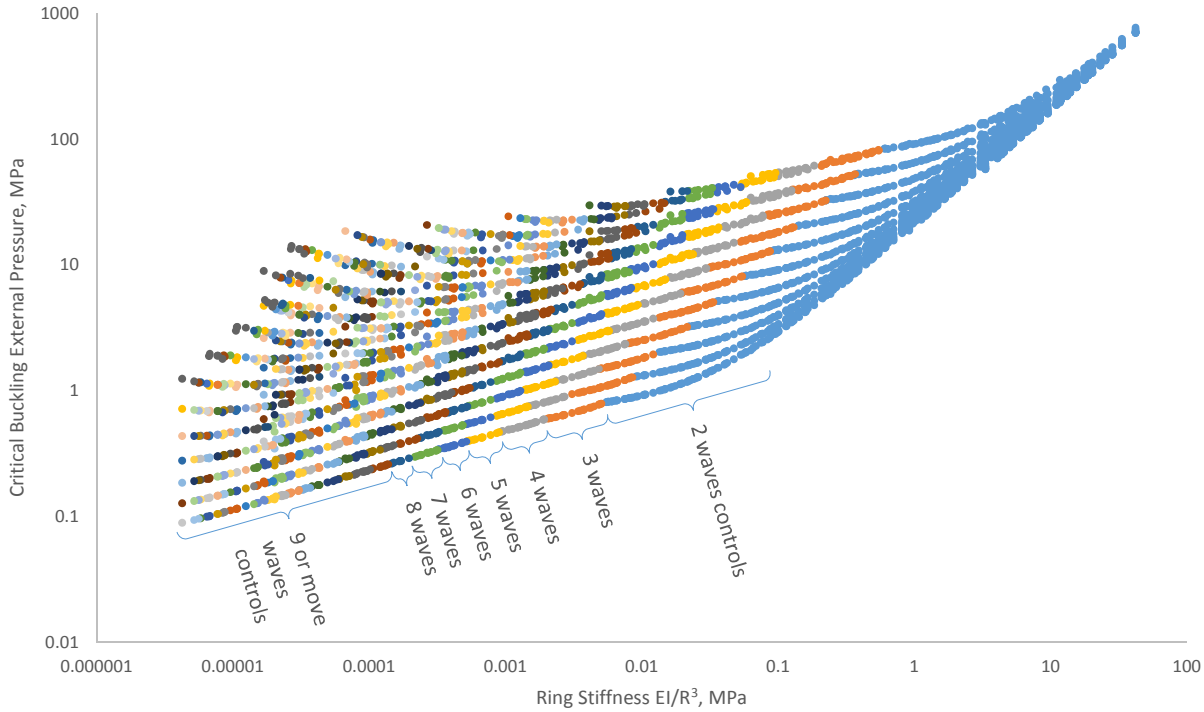

Figure 4 – Critical buckling pressure of circular pipes with elastic soil support, colorized by critical buckling wave number.

The heights were selected to span the responses of gross section yield, plastic buckling, and global elastic buckling of the unsupported column in compression with fixed ends matching the boundary conditions defined in these analyses described below.

Both eigenvalue buckling and nonlinear compression analyses were performed for a shell representation of the profile using four-node linear shell elements S4. Two full corrugations were modeled (Figure 5); one edge of the member remained free, while a symmetry condition was applied to the other edge so that in effect four corrugations were modelled. Each node along the ends of the member was restrained against translation, but allowed to rotate. Although the boundary condition at each node is a pin, locally, rotations of the ends of the cross-section are globally restrained because of the depth of the profile, and the constraint simulates the ends of the profile being welded to rigid caps. Warping is restrained in both ends.

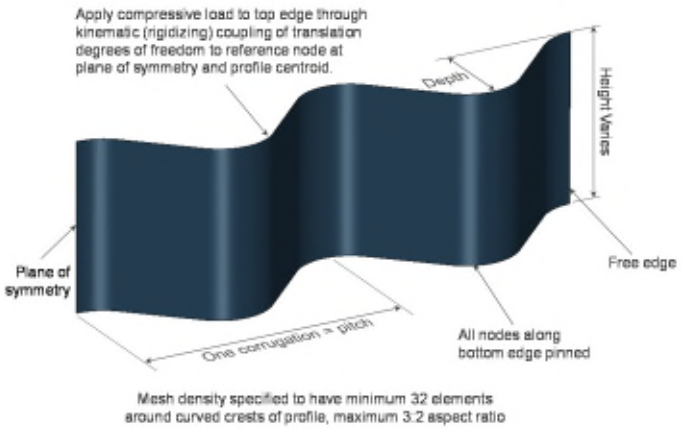

Figure 5 - Model schematic and boundary conditions for compression of straight sections

4.2.1. Linear Elastic Eigenvalue Buckling Analysis

For eigenvalue analysis, the members were loaded in concentric axial compression with a unit load, and the first ten eigenvalue buckling modes were extracted. The critical load for the controlling buckling mode of each analysis is shown in Figure 6 as a fraction of the gross section yield strength. The results show that for an appreciable number of sections evaluated, the critical elastic buckling load controls over gross section yield.

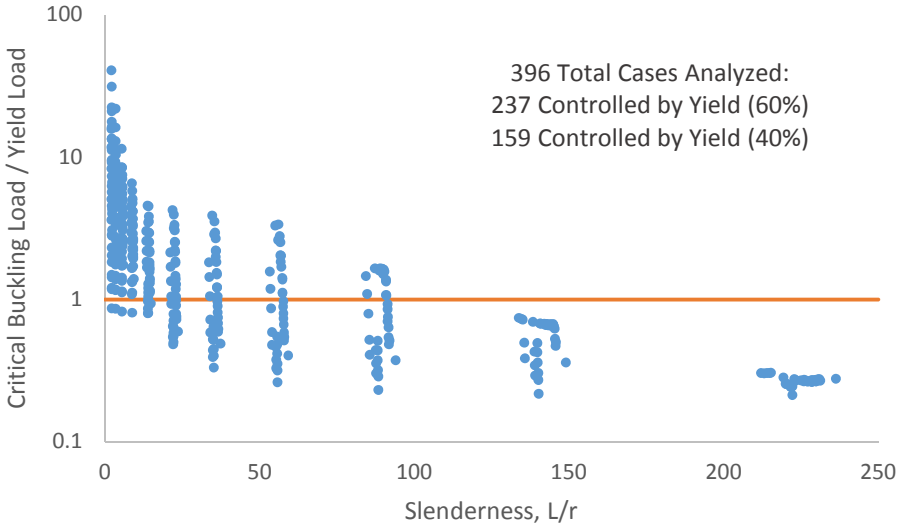

Figure 6 – Critical elastic buckling load as a fraction of yield load, plotted against section slenderness from linear eigenvalue analysis of buckling of straight section.

Recall that the analyses of straight sections do not include soil support. In the previous section, we discussed how the effect of soil support on stability is minimized as the wavelengths decrease, and soil support has

little effect on local and distortional modes compared with its effect on global stability. For example, the mode shapes and critical loads for two eigenvalue buckling analyses of straight sections are shown in Figure 7, with and without support from soil with modulus of subgrade reaction of 40.7 MPa/m (appropriate for soil with elastic modulus of 13.79 MPa). The soil support in these cases is modeled with distributed linear springs, implying that sufficient pre-compression exists to prevent the pipe separating from the soil. For Profile 8, the change in critical load is 12-17% and mode shapes are similar with the exception of closely spaced modes 3 and 4 which exchanged order. For Profile 13, which uses a significantly thicker plate, the differences in critical loads and mode shapes are negligible. Compared with global stability, the effect of soil support on local buckling modes is minimal.

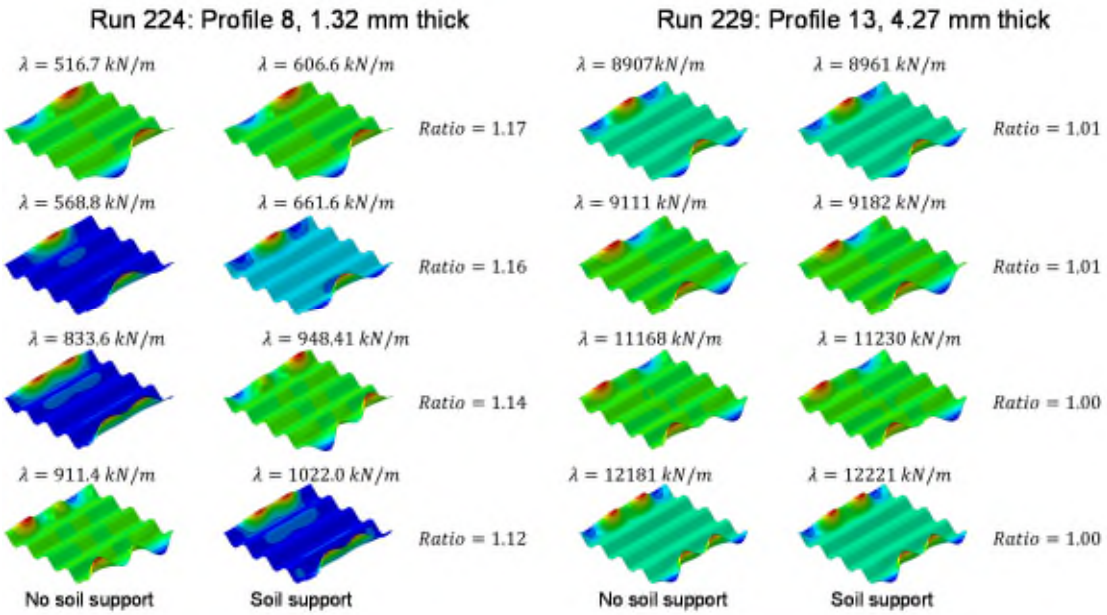

Figure 7 – Effect of soil support on elastic local buckling critical load. Results shown for 76.2 mm pitch × 25.4 mm depth Profiles No. 8 (1.32 mm thickness) and No. 13 (4.27 mm thickness). Contours show lateral deformation. Eigenvalues reported are compressive thrust [kN/m] corresponding to mode shape shown

4.2.2. Nonlinear Compression Analysis

The preceding subsection showed that stability controls over yield in many analysis case. The onset of small local or distortional buckling prior to full section yield may not significantly reduce the compression capacity of the section. We performed nonlinear compression analyses for the same set of straight sections form the previous subsection to determine the peak load carrying capacity of each profile over a range of heights. For nonlinear compression analysis, the model used material plasticity with hardening based on tensile tests run on coupons removed from a corrugated plate sample. The entire corrugated model was analyzed with a single material model based on actual coupon tests which found an average yield strength of 291 MPa. While it is expected that the crests of corrugations will exhibit increased yield strength due to cold working effects, the model did not differentiate between material properties at flats and crests.

The two lowest mode shapes from the attendant eigenvalue analysis were used as seeds to introduce imperfections into the nonlinear compression analyses. The mode shapes were each scaled to have a maximum amplitude of one-half the plate thickness, ensuring that at no point on the member would the imperfection exceed one plate thickness. The intent was not to study the imperfection sensitivity of the system, but to prevent spurious over-estimates of the capacity of the sections and to improve the numerical conditioning of the analyses. Compressive load was applied concentrically to the section. Riks incrementation was used to capture post-peak behavior and collapse of the members in compression.

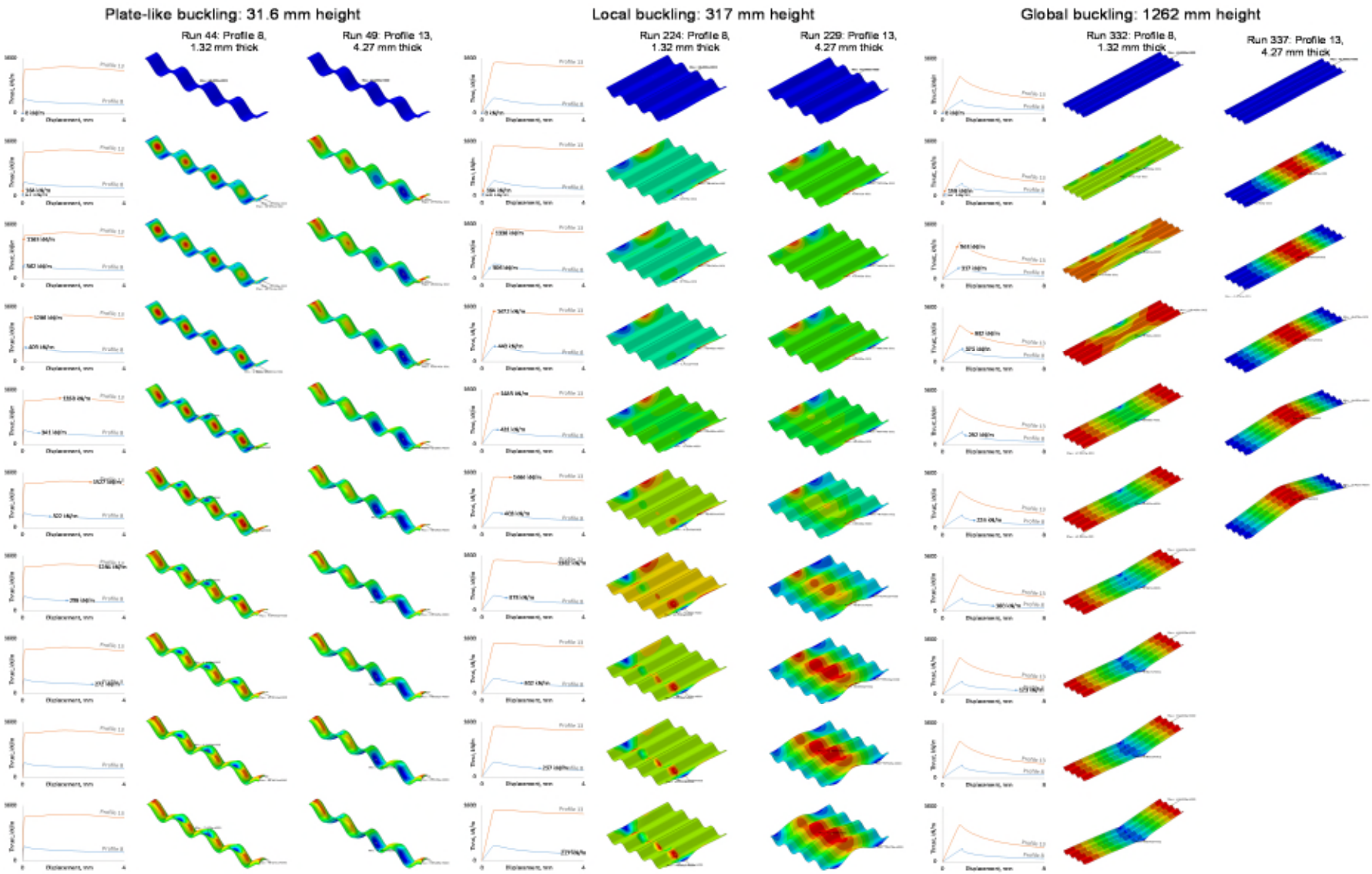

Figure 8 – Deformed shapes for 76.2 mm pitch × 25.4 mm depth Profiles No. 8 (1.32 mm thickness) and No. 13 (4.27 mm thickness). Contours show lateral deformation. Three select heights (31.6 mm, 317 mm, and 1262 mm) are shown to demonstrate different collapse mechanisms: plate-like buckling of short sections, local buckling, and global buckling. Load displacement plots indicate current state of load attendant to each deformed shape.

Figure 8 presents the results from the nonlinear compression analyses of two selected profiles having the same pitch (76.2 mm) and depth (25.4 mm) but differing thickness (1.32 mm and 4.27 mm). The deformed shapes are plotted at multiple increments through the displacement history. Color contours indicate lateral displacement trends but are intentionally not plotted with a common scale to highlight small local deformations and larger global displacements, as appropriate. Load-displacement plots accompany each pair of deformed shape and contour plots and indicate the load and displacement states for the respective analyses. Results are plotted for three selected heights of eleven heights analyzed for both profiles: 31.6 mm, 317 mm, and 1262 mm. The heights were selected to highlight the different collapse mechanisms observed during the analyses. Shorter heights fail in gross-section yield and plate-like buckling of the elements of the profile. Intermediate heights undergo local buckling which triggers crippling and/or global plastic buckling. Larger heights fail by elastic global buckling of the section.

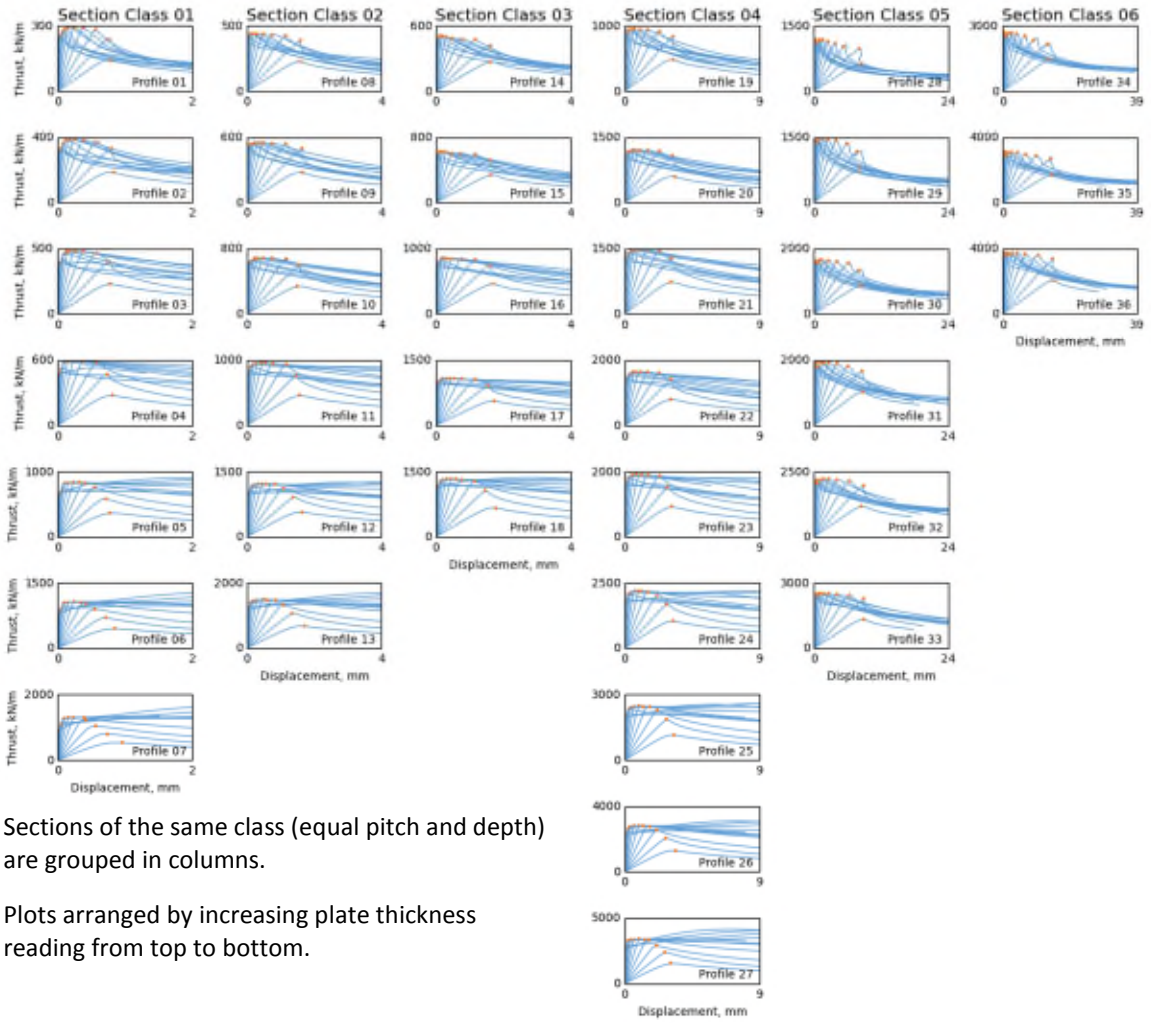

Figure 9 - Load displacement histories for nonlinear compression of profiles. All 11 heights for each profile are plotted. Local maxima identified with orange markers. Each column of plots contains the results for all sections of the same Class (equal pitch and depth) with increasing plate thickness reading down the column of plots.

Figure 9 shows the load-displacement histories for all nonlinear compression runs. Each subplot gives the results for the eleven heights analyzed for that profile. The peak loads are identified with orange markers. In general, as the height of the section increases, the peak load decreases and the displacement at which the peak load occurs increases. While profiles with thin plates exhibit sharp peaks with a rapid decrease in load post-peak (e.g., Profile 8), others with thick plates undergo large ductile deformations without a significant reduction in load (e.g., Profile 13). The difference in response appears to be related to the ratio of the

thickness of the plate to the tangent length (flat length) and likely is related to the local buckling capacity of the section.

The peak loads identified from each analysis were used to calculate the critical average stress for the section with a given slenderness, and those results are plotted in Figure 10. The material yield strength and Euler elastic column buckling limit bound the results, as expected. For slenderness values between 100 and 200, the calculated critical average stress is lower than the envelope of yield strength and the Euler column buckling limit where the sections exhibit failure due to plastic buckling. As a result of the method for selecting the section heights for analysis, the results are clustered at discrete slenderness values. The cause of the spread within each cluster is not known at this time, but are hypothesized to reflect local instabilities particular to each profile that are not represented in the plot over slenderness ratio.

We compared the results from the eigenvalue buckling analysis with the nonlinear compression analyses where the controlling eigenvalue was less than the yield load. The results are shown in Figure 11, and expressed in terms of average stress calculated as compressive thrust divided by the area of the profile. The plot shows general agreement between the elastic and nonlinear analyses, with %-difference ranging between -30/+60% (nonlinear/eigenvalue). Some runs show significant capacity after the onset of local buckling.

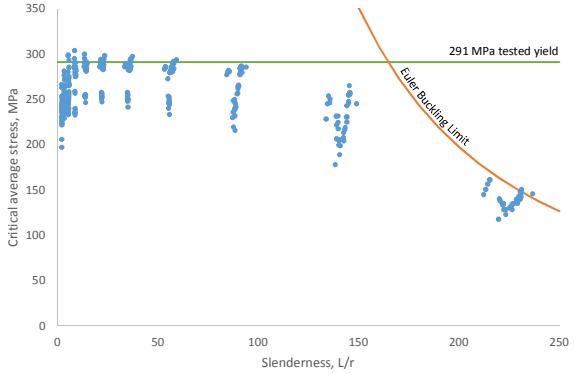

Figure 10 – Critical average stress (critical load divided by profile area) from nonlinear compression analyses versus profile slenderness, L/r. Tested yield strength limits is shown. Euler elastic global buckling limit is plotted for a fixed end condition

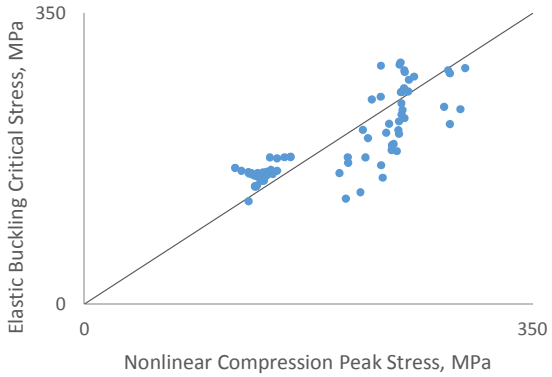

Figure 11 - Critical stress from eigenvalue buckling analysis versus peak stress from nonlinear compression analysis.

.

5. Conclusions

Analyses showed two distinct regimes of behavior for the global stability, depending on the critical number of harmonic waves that form around the circumference (two or greater than two). For configurations where the critical number of harmonic waves is greater than two, the logarithm of the critical buckling pressure varies with the logarithm of the ring bending stiffness, and the logarithm of soil elastic modulus. For configurations where two harmonic waves controls the sensitivity to soil stiffness decreases.

Soil support has a significant effect on global stability of flexible pipes, and relatively little effect on higher frequency buckling local and distortional modes, due to the ratio of strain energy in the soil to the strain energy in the pipe wall. The local and distortional stability of corrugated metal pipe sections can therefore be evaluated without inclusion of the soil support with significant overconservatism. For thicker plates, the effect of soil support on local and distortional modes is even less.

The post-buckling behavior is a function of the plate thickness. For thin plates the peak in the load-displacement curve is sharp and pronounced, with significant reduction in load carried post-buckling. For thicker plates, the post-peak response can be very ductile, and even show additional post-buckled capacity.

6. Future Research

In performing this study, we identified several areas for further research:

- Only nominal imperfections were included in the present study. To facilitate the large number of analyses performed, the first two Eigen buckling modes were independently scaled to have a maximum amplitude of one-half the plate thickness and introduced as imperfections to the nonlinear compression analyses of straight sections. A detailed study of the effect of imperfections on the capacity of CMP sections that includes information on fabrication and installation tolerances should be made to properly evaluate the capacity of installed pipes.
- Large diameter CMP and culvert installations are often manufactured from multiple arc segments with longitudinal and circumferential single lap bolted seams. The single lap connections introduce local bending and yielding in the plate near the connection, and the effect of which on the stability of CMP warrants additional study and could readily be introduced into the analyses of straight sections presented here.
- The increased yield strength in the crests of the profiles and residual stresses from cold working were not included in the nonlinear compression analyses. The effects of cold working on the results presented here should be investigated.
- The buckling mode shapes calculated for straight sections could be classified according to global, local, and distortional modes to better understand the interaction between buckling modes. Direct strength analysis by CUFSM would also add to the understanding of the stability of corrugated profiles.
- The analyses for global stability were performed on 2D circular sections of varying diameters with equivalent ring bending stiffness and varying soil support, while the analyses for local and distortional stability were performed on straight corrugated sections of varying lengths. To compare the results of the global stability models with those for local and distortional stability it is necessary to select the appropriate height for the analyses of straight sections that corresponds to the global stability analyses. Three dimensional eigenvalue buckling analyses of circular sections with corrugated profiles, and introduction of soil support to the analyses of straight sections could support this work.
- Detailed interaction between buried CMP and the surrounding soil, including pipe-soil friction, separation, backfill compaction, soil nonlinearities, and other phenomena should be incorporated into the analyses. The analysis results should also be compared with experimental data.

References

Abaqus v6.14 software documentation, Dassault Systèmes Simulia Corp., Providence, RI, USA, 2014.

AASHTO (2014), *AASHTO LRFD Bridge Design Specifications*, Customary U.S. Units, 7th Edition)

ASTM International (2015). ASTM A796 Standard Practice for Structural Design of Corrugated Steel Pipe, Pipe-Arches, and Arches for Storm and Sanitary Sewers and Other Buried Applications.

CHBDC (2006), CSA-S6: *Canadian Highway Bridge Design Code*, Canada

Brown, M. J., Moore, I. D., & Fam, A. (2014). Performance of a cured-in-place pressure pipe liner passing through a pipe section without structural integrity. *Tunnelling and Underground Space Technology, 42*, 87-95.

Duns, C. S., & Butterfield, R. (1971, November). Flexible buried cylinders: Part III—Buckling behaviour. In *International Journal of Rock Mechanics and Mining Sciences & Geomechanics Abstracts* (Vol. 8, No. 6, pp. 613-627). Pergamon.

García, D. B., & Moore, I. D. (2015). Performance of deteriorated corrugated steel culverts rehabilitated with sprayed-on cementitious liners subjected to surface loads. *Tunnelling and Underground Space Technology*, *47*, 222-232.

Luscher, U., "Buckling of Soil-Surrounded Tubes." Journal of Soil Mechanics Foundation Division, Proceedings of the American Society of Civil Engineers, Vol. 92, No. SM6 (Nov. 1966) pp. 211–2218.

Moore, I. D. (1989). Elastic buckling of buried flexible tubes-a review of theory and experiment. *Journal of geotechnical engineering*, *115*(3), 340-358.

Moore, I. D., Haggag, A., & Selig, E. T. (1994). Buckling strength of flexible cylinders with nonuniform elastic support. *International journal of solids and structures*, *31*(22), 3041-3058.

National Corrugated Steel Pipe Association (2008), *Corrugated Steel Pipe Design Manual*, 2nd Edition

McGrath, T.J., I.D. Moore, E.T. Selig, M.C. Webb, B. Talen (2002). *NCHRP Report 473: Recommended Specifications for Large-Span Culverts*. National Academy Press, Washington DC,

Trickey, S. A., Moore, I. D., & Balkaya, M. (2016). Parametric study of frost-induced bending moments in buried cast iron water pipes. *Tunnelling and Underground Space Technology*, *51*, 291-300.

Uckan, E., Akbas, B., Shen, J., Rou, W., Paolacci, F., & O'Rourke, M. (2015). A simplified analysis model for determining the seismic response of buried steel pipes at strike-slip fault crossings. *Soil Dynamics and Earthquake Engineering*, *75*, 55-65.

Wilson, D., Filion, Y. R., & Moore, I. D. (2015). Identifying Factors that Influence the Factor of Safety and Probability of Failure of Large-diameter, Cast Iron Water Mains with a Mechanistic, Stochastic Model: A Case Study in the City of Hamilton. *Procedia Engineering*, *119*, 130-138.

Zhang, B., Ye, C., Liang, B., Zhang, Z., & Zhi, Y. (2014). Ductile failure analysis and crack behavior of X65 buried pipes using extended finite element method. *Engineering Failure Analysis*, *45*, 26-40.